Hydroxylation of the surface of PbS nanocrystals passivated with oleic acid

Danylo Zherebetskyy[1], Marcus Scheele[1,2], Yingjie Zhang[1,3], Noah Bronstein[2], Christopher Thompson[1,2], David Britt[4], Miquel Salmeron[1], Paul Alivisatos[1,2], Lin-Wang Wang[1,*]

1Materials Sciences Division, Lawrence Berkeley National Laboratory, Berkeley, CA 94720, USA.

2Department of Chemistry, University of California at Berkeley, Berkeley, CA 94720, USA.

3Applied Science and Technology Graduate Program, University of California at Berkeley, Berkeley, CA 94720, USA.

4The Molecular Foundry, Lawrence Berkeley National Laboratory, One Cyclotron Road, Berkeley, CA 94720, USA.

↲*Corresponding author. E-mail: lwwang@lbl.gov

Science 29 May 2014:

DOI: 10.1126/science.1252727

Article

Abstract

Controlling the structure of colloidal nanocrystals (NCs) is key to the generation of their complex functionality. This requires an understanding of the NC surface at the atomic level. The structure of colloidal PbS-NC passivated with oleic acid has been studied theoretically and experimentally. We show the existence of surface OH- groups, which play a key role in stabilizing the PbS(111) facets, consistent with x-ray photoelectron spectroscopy as well as other spectroscopic and chemical experiments. The role of water in the synthesis process is also revealed. Our model, along with the existing observations of NC surface termination and passivation by ligands, helps to explain and predict the properties of NCs and their assemblies.

The structure of the interior of nanocrystals (NCs) can be determined quite accurately by crystallography, but the structure of their surfaces cannot be obtained from this analysis due to the complexity of organic capping ligands (*1*–*6*). However, the NC surface structure controls the growth and solubility, and strongly influences the physical and chemical properties (*7*–*12*). We take advantage of improved insights of the mechanisms of nanocrystal growth (*3*–*6*), combined with extensive ab initio total energy calculations, to create a testable model for the atomic surface passivation structure of the exposed facets of a PbS-NC. The model makes specific, and at first surprising, predictions about the surface-bound species that were subsequently verified experimentally. PbS is ideal for this study because of the high symmetry of its rocksalt structure and its propensity to form NCs with well-defined (111) and (001) facets (*13*, *14*). PbS-NCs with controlled size and shape can be produced from a PbO lead precursor, hexamethyldisilathiane (TMS2S) sulfur precursor, and oleic acid that binds to exposed Pb atoms to stabilize the surface (*1*–*6*).

We performed ab initio electronic structure calculations on relevant sub-systems and on the reaction steps involved in the synthetic process, including: studies of immediate

precursors; fate of by-products of the initial decomposition step; NC-ligand interactions; and ligand-ligand and ligand-solvent interactions. Our methods (*15*) are density functional theory (DFT) in the generalized gradient approximation (GGA). The GGA is not accurate enough to describe the van der Waals (vdW) interactions, and the entropic contributions in the solvent are prohibitively time-consuming at present to be calculated directly. However, we have taken advantage of likely cancellations of these terms when comparing different systems. We found the following features in our theoretically derived model: (1) The Pb:S atomic ratio is roughly 1.2:1 (Pbexcess:S~0.2:1) for ~5 nm NCs; (2) The ratio between the number of surface oleate molecules and the number of excess Pb atoms is ~1:1; (3) The ligands can be easily removed from the (001) surface; (4) The average (111)/(001) surface to center distance ratio of the truncated octahedral shape is about 0.82:1; (5) OH- groups are present on the NC (111) facet. These features are consistent with prior and current experimental studies including Rutherford backscattering (RBS), TEM (TEM), X-ray photoelectron spectroscopy (XPS), sum frequency generation (SFG) spectroscopy, nuclear magnetic resonance (NMR), and Fourier transform infrared spectroscopy (FTIR) (*5*, *6*, *16*–*18*). The presence of hydroxide groups on the surface predicted in the calculation as by-products of precursor decomposition was verified with XPS and SFG. The existence of water in the precursor was supported with NMR and FTIR measurements.

The colloidal PbS-NCs (*4*, *5*) are synthesized by dissolving PbO in hot oleic acid (*15*). One of the by-products of the reaction is water, which was proposed to remain as free molecules in the solution (*4*, *5*). Our calculations however show that it is energetically more favorable for water to bind to the Pb-precursor (*15*). Thus, the first reaction step can be written as:

$$PbO + 2 \cdot OAH \rightarrow Pb(OA)_2 \cdots H_2O$$

(1)

where OAH denotes oleic acid. The DFT optimized structure of the Pb(OA)2···H2O is shown in Fig. 1A. In the experiment, the reaction products were degassed at 110°C under vacuum for 1 hour. To determine whether such degassing removed all of the water in the precursor as previously suggested, we used NMR and FTIR. Although NMR demonstrated the absence of liquid water, it was unable to distinguish water molecules bound to the Pb(OA)2 complexes (*15*). Using FTIR measurements and deuterated oleic acid (d1-OA), we distinguished O-H stretching modes associated with water bound to Pb(OA)2 (*15*). The d1-OA was prepared so that only the acid H was exchanged for D. A major part of the water remained after degassing in sufficient amounts to provide the required 20% of water in Eq. 1 for the surface passivation described below (Pbexcess:S = 0.2:1, one OH- per excess Pb). The existence of water is consistent with the observation that the Pb(OA)2 precursors often form clusters (*19*). As a further demonstration of the role of water we added acetic anhydride (*20*), as a drying agent during the reaction of Eq. 1, followed by evacuation to remove acetic acid and excess anhydride (*15*). The subsequent formation of PbS-NC was much slower and the NCs were of reduced size, from the 8 to 10 nm (for that particular synthesis condition) to 4 nm. Also, the particle shapes became rather irregular with many (001) surfaces (*15*), consistent with our model.

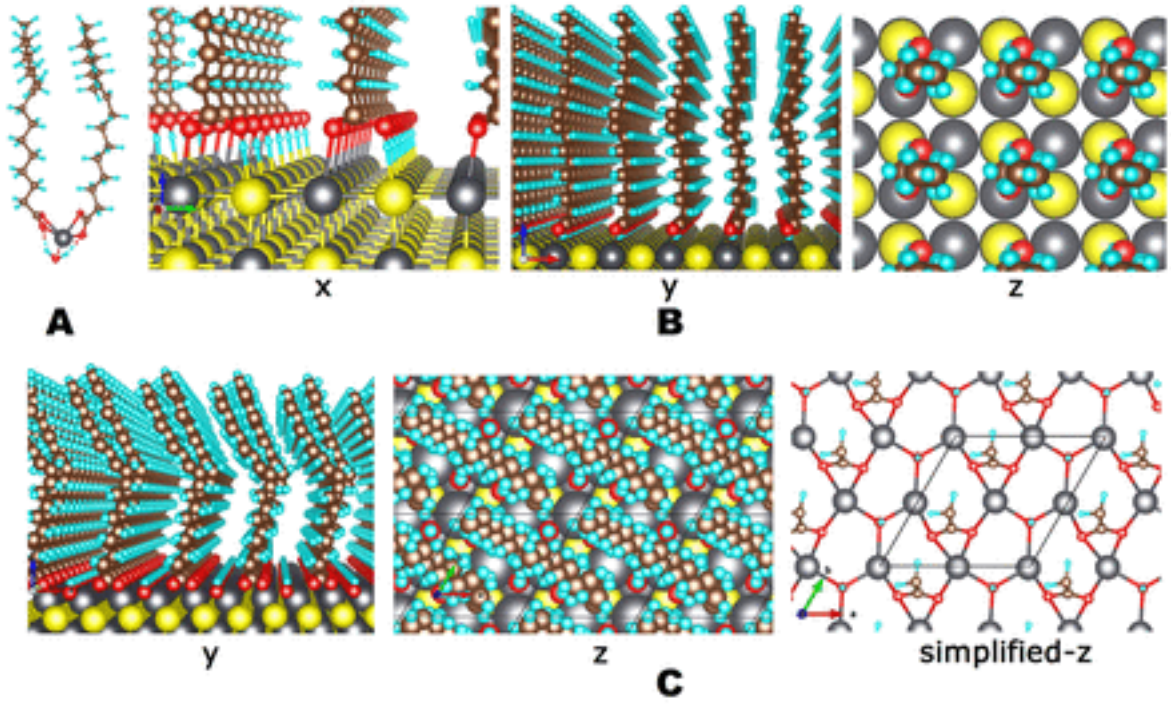

Fig. 1
Optimized molecular configurations.
(A) A water molecule formed during NC synthesis is bound to the Pb(OA)2 molecule forming a Pb(OA)2···H2O complex. (B) Relaxed configuration of OAH molecules on the PbS(001) surface (x,y,z-views). (C) Relaxed lowest energy configuration of OA- and OH- molecules on the PbS(111) surface: y- and z-views. On the right a simplified z-view schematic is shown with truncated tail chains. Pb(gray), S(yellow), O(red), H(blue), C(brown).

In the second step, TMS2S dissolved in trioctylphosphine (TOP) is injected into the heated Pb(OA)2···H2O precursor dissolved in octadecene:

$$Pb(OA)_2 \cdots H_2O + (TMS)_2S \rightarrow PbS + (TMS)_2O + 2 \cdot OAH$$

(2)

The calculated ΔG of Eq. 2 is -2.13 eV. It was suggested that the end product from oleic acid is (oleyl-CO)2O (*4*, *5*). It is also known, and computationally confirmed, that water will react with (oleyl-CO)2O to form two oleic acid molecules. Thus, during NC synthesis, oleic acid, Pb(OA)2···H2O (from excess Pb(OA)2 precursor), (TMS)2O, TOP and octadecene are present in the solution as possible passivants. In the following, we will consider passivations of the (001) and (111) surfaces separately.
Our calculation shows that oleic acid has the strongest binding energy to the (001) surface, because of its -COOH group (*15*). The (001) surface covered by OA- (*9*) has a much higher energy than when covered by OAH, because the OA- can bind with a cation in the solvent, and thus has a much lower chemical potential in the solvent than OAH. On the PbS (001) surface, the -COOH groups form bidentate bridges between Pb and S

atoms (–C=O···Pb and -COH···S bonds; Fig. 1B). This model contains one OAH molecule per two surface PbS-pairs: one pair bound to one OAH, and the other unbound. A high-density packing, with one OAH per PbS-pair, is unfavorable because of steric repulsions between the oleyl tails. The binding energy between oleic acid and the PbS-(001) surface is calculated as:

$$E(bind) = E(mol/surf) - (E(mol) + E(surf))$$

(3)

Here E(mol/surf) is the energy of the whole system, E(surf) is the energy of the unpassivated nonpolar PbS(001) surface after atomic relaxation, and E(mol) is the free energy of the passivating molecule in the solvent including solvent binding effects. There are two types of solvent binding effects, hydrogen-bonding (H-bonding) between functional groups and vdW interactions between alkane chains; of these, only H-bonding can be described accurately by the GGA method. For the vdW interaction, we have removed the GGA vdW alkyl chain-chain interaction energy from the E(mol/surf) term in Eq. 3 because the chain-chain vdW interaction will approximately cancel each other between the E(mol/surf) term and E(mol) term (*15*). For E(mol), we included the –0.83 eV binding energy of the H-bonded OAH-OAH dimer. We also ignored the entropy change of the ligand molecules, which we deem to be small (*15*). The final calculated (001) binding energy is –0.16 eV per oleic acid (Table 1).

Table 1

Surface and ligand binding energies for the (001) and (111) surfaces of PbS-NC. The (001) and (111) surface areas per OAH (OA-) molecule are 35.2 Å2 and 30.5 Å2 respectively.

Assessing the energetics of capping the polar (111) facets is more complicated because of the need for charge compensation (*21*, *22*) to satisfy the electron counting rule (*23*–*25*). The NCs formed in Eq. (2) have equal number of Pb and S, with stoichiometric nonpolar (111) facets with only half of the terminal Pb atoms (*22*, *26*). We then considered whether the Pb(OA)2···H2O group in the solvent can fill-in the surface vacancies (missing Pb atoms). We found that, in agreement with Bealing *et al*. (*9*), it is sterically impossible to fill every missing Pb atom of the (111) surface with one Pb(OA)2, but one OA- per missing Pb is possible. Hence an anionic species is needed for charge balance. This species is OH-, provided by the dissociation of bound H2O, while the H+ is used to form OAH

$$(PbS)_N(111) + Pb(OA)_2 \cdots H_2O \rightarrow OA - Pb_{N+1}S_N(111) - OH + OAH$$

(4)

Here (PbS)N(111) denotes the reconstructed nonpolar (111) surface and PbN+1SN(111) denotes the full Pb-terminated polar surface (Fig. 2, A to D). The binding energy of this passivation, which equals to the ΔG of the reaction (4), is –0.52 eV per oleate (Table 1), which is much larger than the (001) surface binding energy. The minimum energy

configuration (*15*) of OA-PbN+1SN(111)-OH is shown in Fig. 1C, where the OA- group stabilizes the Pb ions via μ2-bidentate bridging bonds and the OH- group stabilizes the Pb ions via μ3-Pb3–OH bonds. In the calculation of ΔG we included the OAH-OAH dimer interaction of –0.83 eV, and removed the alkyl chain-chain vdW interaction at the surface like in the (001) surface case. Although we have considered other possible passivation stoichiometries and configurations (*15*), none was found to be as stable as the ones considered above (Table 2).

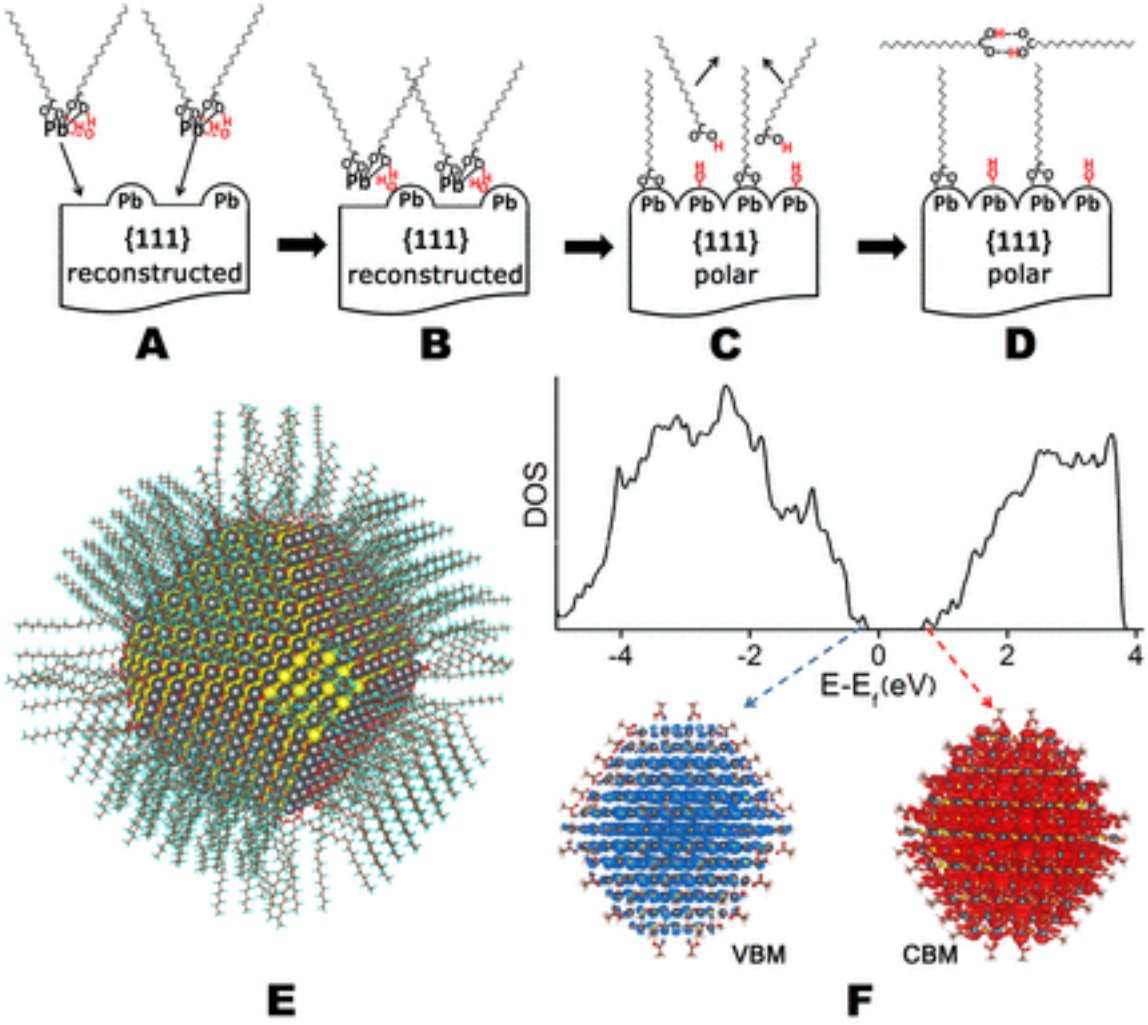

Fig. 2
Model of PbS-NC in colloidal solution. (A-D) Multistep process for building up the (111) facets of PbS-NC: (A) Pb(OA)2···H2O precursors approach the nonpolar and stoichiometric (111) facets. (B) Pb ions bind to surface vacancies. (C) One of the two OA- in each Pb(OA)2···H2O complex is removed due to steric effects, and the water molecule dissociates to provide an OH- group to the surface, and H+ for desorbing OA-. (D) The desorbed OAH molecules dimerize in the solvent. (E) Calculated atomic structure of a 5nm diameter NC passivated with OA- and OH- ligands [coordinates in (*15*)]. (F) Electron density of states, showing the valence band maximum (VBM) and conduction band minimum (CBM) levels, of a NC passivated with truncated oleic acid alkyl chains [coordinates in (*15*)].

Table 2 Ligand patterns binding energies (eV) on the (111) PbS-NC surface for a 4 Pb atoms area.
For Pb(OA)2 cases, the binding energy of H2O with Pb(OA)2 and the binding of liquid water (after Pb(OA)2 is bound to the surface) are taken into account. The "2OA-, 2OH-" (current model) value is twice that shown in Table 1 because the surface area is twice as large here. The "2OA-, O2- " corresponds to the case where 2OH- form one O2- on the surface and one H2O leaving the surface.

View this table:

In order to predict the shape of the PbS-NC, we calculated the surface energies of the (001) and (111) surfaces, which are equal to the unpassivated surface energies (nonpolar for (111)) plus the binding energies calculated above. The unpassivated surface energies were calculated from the energies of the slabs minus the corresponding bulk values. The resulting energies (Table 1) were used in a Wulff construction model (*27*–*29*) to determine the equilibrium NV shape. We obtain a (001) to (111) Wulff ratio of 0.82, in excellent agreement with the average 0.82 value derived from TEM images (Fig. 3). With this procedure we constructed a model NC with all the surface passivation features (*15*) and with OH- groups placed at the edges to determine if it provides good passivation of edges and corners. To simplify the calculation we truncated the alkyl chains of the oleic acids to the shorter acetic acid, which is not expected to change NC surface electronic structure. We subsequently relaxed the atomic structure of the 2325 atoms, 4 nm diameter NC in the DFT/GGA (*15*). The final system shows perfect surface passivation, with a clean band gap, without impurity or defect induced states (Fig. 2F), and with good edge and corner passivation. Thus, we propose that the 3D bulk structure determines the 2D surface passivation structure, which in turn determines the 1D edge passivation. For a 5 nm NC, our model (*15*) also provides the ratio between excess-Pb and S atoms of 0.19:1, and between excess-Pb and surface OA molecules of 1.18:1 respectively, which agree closely with experimentally observed values of 0.21:1 (measured by RBS) and 0.97:1 reported in (*6*). In our model the ligand binding energy on the (001) surface is much smaller than that on the (111) surface, consistent with the images in Fig. 3, where all NC are standing up on (001) facets, with some in direct contact via (001) facets. Both observations indicate that it is easy to remove the ligand molecules from the (001) facets.

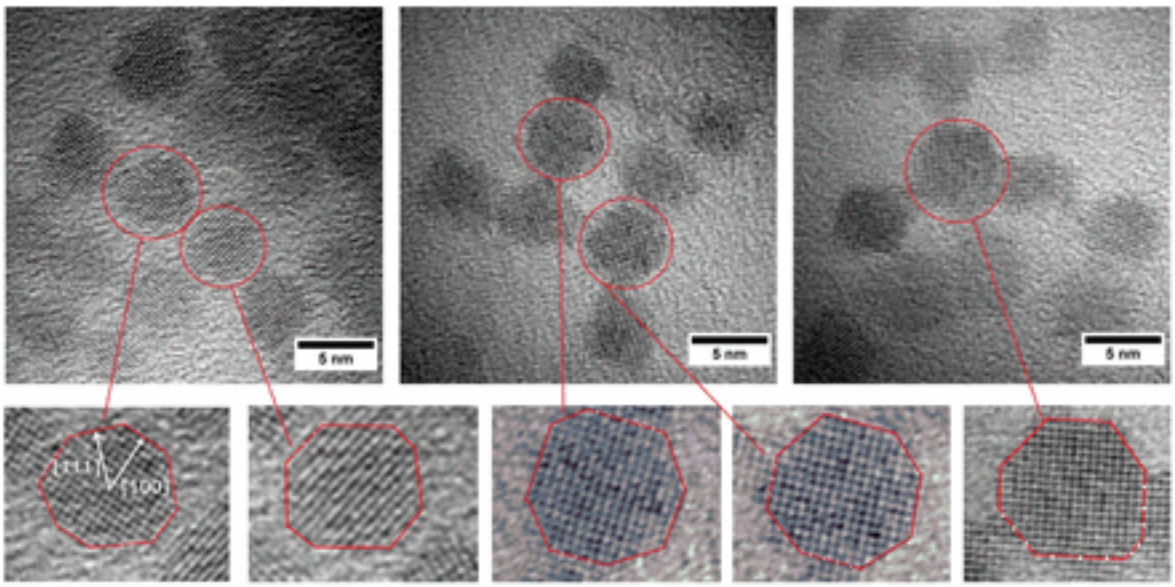

Fig. 3
TEM images of PbS-NCs.
High-resolution TEM images of the synthesized PbS-NC with enlarged views of selected NC shown below. The (111)/(001) Wulff ratios of center-to-surface distances of NCs are 0.820, 0.762, 0.866, 0.847, 0.792 from left to right, respectively, with an average ratio of 0.817, in good agreement with the calculated value.

One of the most interesting features of our passivation model is the existence of the OH- groups on the (111) facet. Water readily dissociates into OH- and H+ on transition metal or oxide surfaces (*30*–*33*), and the binding of H2O to Pb(OA)2 in the solvent provides a natural kinetic pathway for this reaction (Fig. 2, A to D). The presence of small size anions is also required to establish charge neutrality over the entire quantum dot that could not be achieved by the sterically hindered OA- molecules alone. The co-existence of sterically demanding ligands, like OA-, and small anions to fill the gaps and fulfill the electron counting rule, could apply to other metal chalcogenide systems as well.
To probe the existence of OH-, two NC samples were synthesized, one as described above (denoted as PbS-OH), and another following the procedure developed by Moreels *et al*. (*17*) that uses Cl- and no water during synthesis [denoted as PbS-Cl (*15*)]. In the PbS-Cl sample, the Cl- anion has effectively replaced OH-. Both samples were spin coated on freshly cleaved graphite, followed by thorough washing with acetone to remove unbound ligands, to form a sub-monolayer film. The XPS data including those for the two control samples, graphite and Pb(OH)2 powder, are shown in Fig. 4. Although the graphite is freshly cleaved in an Ar glove box (with less than 1 ppm oxygen concentration), it is slightly oxidized (*34*, *35*), showing an O 1s peak at 534.0 eV. Because of the incomplete surface coverage (*15*), this substrate peak is also present in the PbS-Cl and PbS-OH NC samples. After subtracting this peak, the PbS-Cl shows only one additional peak at 532.1 eV, likely from the oleate species. The PbS-OH sample contains three peaks at 534.0 eV, 532.1 eV, and 531.2 eV. The new peak at 531.2 eV is assigned to OH-, in agreement with the Pb(OH)2 powder single peak at 531.2 eV, and with reported values for other metal-OH groups XPS peaks (*36*, *37*). In the PbS-Cl sample, this feature is absent while the chlorine species produced a peak in the XPS (*15*). We note

that the 534.0 eV and 532.1 eV peaks have the same widths in different samples in Fig. 4. The SFG measurement also indicates the existence of OH- in the sample (*15*). While the present work applies to PbS-NC, we expect the general applicability of this approach to other colloidal NCs.

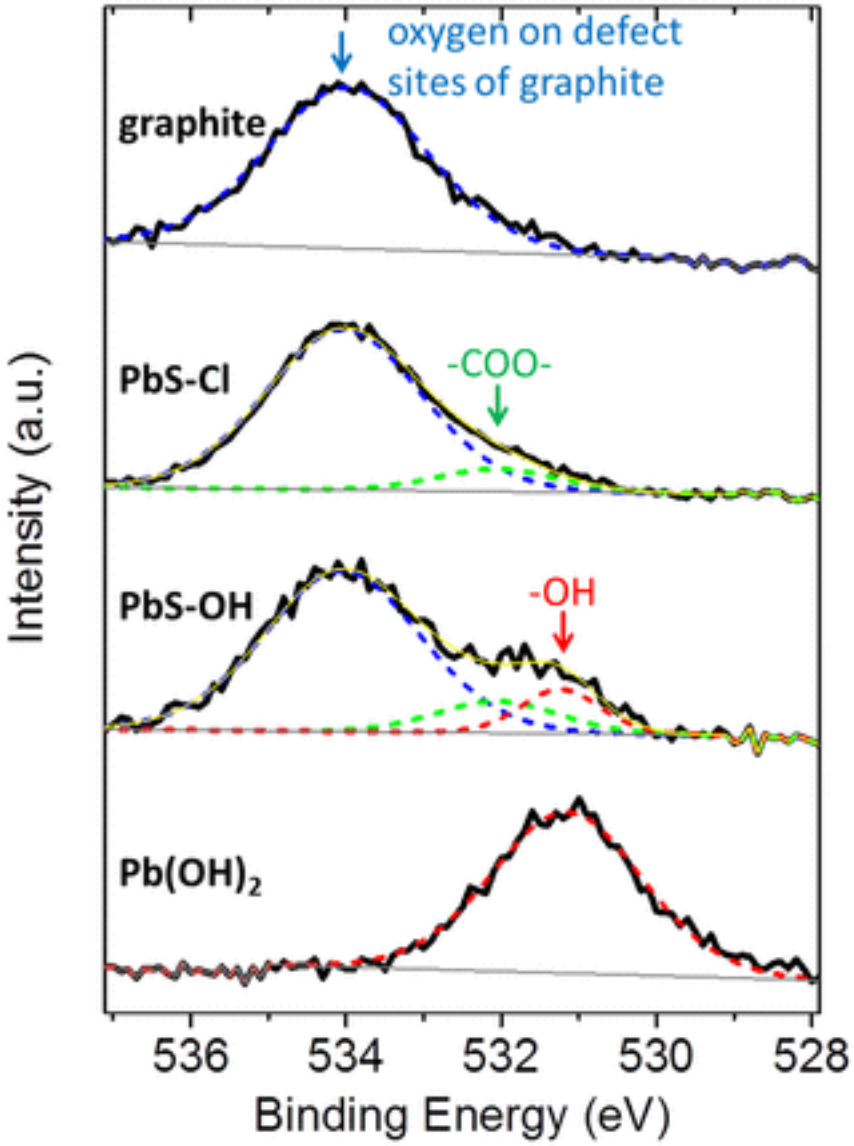

Fig. 4
The XPS spectra of PbS-NCs.
O 1s XPS showing peaks at 531.2eV (red) from oxygen in OH- groups, and at 532.1eV (green) from oxygen in carboxyl groups. The peak at 534 eV is due to substrate O bound to graphite.

Supplementary Materials
www.sciencemag.org/cgi/content/full/science.1252727/DC1
Materials and Methods
Supplementary Text
Figs. S1 to S19

Tables S1 to S3
References (*38*–*83*)
Databases S1 and S2

References and Notes

1 1 ↵P. Alivisatos, Semiconductor clusters, nanocrystals, and quantum dots. *Science* 271, 933–937 (1996). doi:10.1126/science.271.5251.933

2 1 B. Murray, S. Sun, W. Gaschler, H. Doyle, T. A. Betley, C. R. Kagan, Colloidal synthesis of nanocrystals and nanocrystal superlattices. *IBM J. Res. Develop*. 45, 47–56 (2001). doi:10.1147/rd.451.0047

3 1 ↵Y. Yin, A. P. Alivisatos, Colloidal nanocrystal synthesis and the organic-inorganic interface. *Nature* 437, 664–670 (2005). doi:10.1038/nature04165 pmid:16193041

4 1 ↵J. S. Steckel, B. K. Yen, D. C. Oertel, M. G. Bawendi, On the mechanism of lead chalcogenide nanocrystal formation. *J. Am. Chem. Soc*. 128, 13032–13033 (2006). doi:10.1021/ja062626g pmid:17017765

5 1 ↵H. Liu, J. S. Owen, A. P. Alivisatos, Mechanistic study of precursor evolution in colloidal group II-VI semiconductor nanocrystal synthesis. *J. Am. Chem. Soc*. 129, 305–312 (2007). doi:10.1021/ja0656696 pmid:17212409

6 1 ↵I. Moreels, B. Fritzinger, J. C. Martins, Z. Hens, Surface chemistry of colloidal PbSe nanocrystals. *J. Am. Chem. Soc*. 130, 15081–15086 (2008). doi:10.1021/ja803994m pmid:18928251

7 1 ↵J. Li, L. W. Wang, Shape effects on electronic states of nanocrystals. *Nano Lett*. 3, 1357–1363 (2003). doi:10.1021/nl034488o

8 1 J. Schrier, L. W. Wang, Shape dependence of resonant energy transfer between semiconductor nanocrystals. *J. Phys. Chem. C* 112, 11158–11161 (2008). doi:10.1021/jp800489m

9 1 ↵C. R. Bealing, W. J. Baumgardner, J. J. Choi, T. Hanrath, R. G. Hennig, Predicting nanocrystal shape through consideration of surface-ligand interactions. *ACS Nano* 6, 2118–2127 (2012). doi:10.1021/nn3000466 pmid:22329695

10 1 L. Klein, R. Roth, A. K. L. Lim, A. P. Alivisatos, P. L. McEuen, *Nature* 389, 699 (1997). doi:10.1038/39535

11 1 D. V. Talapin, J. S. Lee, M. V. Kovalenko, E. V. Shevchenko, Prospects of colloidal nanocrystals for electronic and optoelectronic applications. *Chem. Rev*. 110, 389–458 (2010). doi:10.1021/cr900137k pmid:19958036

12 1 ↵A. H. Ip, S. M. Thon, S. Hoogland, O. Voznyy, D. Zhitomirsky, R. Debnath, L. Levina, L. R. Rollny, G. H. Carey, A. Fischer, K. W. Kemp, I. J. Kramer, Z. Ning, A. J. Labelle, K. W. Chou, A. Amassian, E. H. Sargent, Hybrid passivated colloidal quantum dot solids. *Nat. Nanotechnol*. 7, 577–582 (2012). doi:10.1038/nnano.2012.127 pmid:22842552

13 1 ↵Y. W. Jun, J. H. Lee, J. S. Choi, J. Cheon, Symmetry-controlled colloidal nanocrystals: nonhydrolytic chemical synthesis and shape determining parameters. *J. Phys. Chem. B* 109, 14795–14806 (2005). doi:10.1021/jp052257v pmid:16852873

14 1 ↵S.-M. Lee, Y. W. Jun, S.-N. Cho, J. Cheon, Single-crystalline star-shaped nanocrystals and their evolution: programming the geometry of nano-building blocks. *J. Am. Chem. Soc*. 124, 11244–11245 (2002).

doi:10.1021/ja026805j pmid:12236719
15 ↵Materials and methods are available as supplementary materials on *Science* Online.
16 1 ↵I. Moreels, K. Lambert, D. De Muynck, F. Vanhaecke, D. Poelman, J. C. Martins, G. Allan, Z. Hens, Composition and size-dependent extinction coefficient of colloidal PbSe quantum dots. *Chem. Mater.* 19, 6101–6106 (2007). doi:10.1021/cm071410q
17 1 ↵I. Moreels, Y. Justo, B. De Geyter, K. Haustraete, J. C. Martins, Z. Hens, Size-tunable, bright, and stable PbS quantum dots: A surface chemistry study. *ACS Nano* 5, 2004–2012 (2011). doi:10.1021/nn103050w pmid:21355621
18 1 ↵V. Petkov, I. Moreels, Z. Hens, Y. Ren, PbSe quantum dots: Finite, off-stoichiometric, and structurally distorted. *Phys. Rev. B* 81, 241304 (2010). doi:10.1103/PhysRevB.81.241304
19 1 ↵D. Britt, Y. Yoon, P. Ercius, T. D. Ewers, A. P. Alivisatos, Hexameric octahedral clusters of PbSe nanocrystals grown from amorphous lead(II) carboxylate nanoparticles. *Chem. Mater.* 25, 2544–2548 (2013). doi:10.1021/cm401083g
20 1 ↵A. J. Houtepen, R. Koole, D. Vanmaekelbergh, J. Meeldijk, S. G. Hickey, The hidden role of acetate in the PbSe nanocrystal synthesis. *J. Am. Chem. Soc.* 128, 6792–6793 (2006). doi:10.1021/ja061644v pmid:16719451
21 1 ↵Y. Gai, H. Peng, J. Li, Electronic properties of nonstoichiometric PbSe quantum dots from first principles. *J. Phys. Chem. C* 113, 21506–21511 (2009). doi:10.1021/jp905868f
22 1 ↵K. Shiraishi, A new slab model approach for electronic structure calculation of polar semiconductor surface. *J. Phys. Soc. Jpn.* 59, 3455–3458 (1990). doi:10.1143/JPSJ.59.3455
23 1 ↵P. Srivastava, Theory of semiconductor surface reconstruction. *Rep. Prog. Phys.* 60, 561–613 (1997). doi:10.1088/0034-4885/60/5/002
24 1 L. Manna, L. W. Wang, R. Cingolani, A. P. Alivisatos, First-principles modeling of unpassivated and surfactant-passivated bulk facets of wurtzite CdSe: A model system for studying the anisotropic growth of CdSe nanocrystals. *J. Phys. Chem. B* 109, 6183–6192 (2005). doi:10.1021/jp0445573 pmid:16851684
25 1 ↵C. Fang, M. A. van Huis, D. Vanmaekelbergh, H. W. Zandbergen, Energetics of polar and nonpolar facets of PbSe nanocrystals from theory and experiment. *ACS Nano* 4, 211–218 (2010). doi:10.1021/nn9013406 pmid:20099911
26 1 ↵K. Kimura, K. Nakajima, Y. Fujii, M. Mannami, Observation of the PbSe(111) surface using high-resolution Rutherford backscattering spectroscopy. *Surf. Sci.* 318, 363–367 (1994). doi:10.1016/0039-6028(94)90110-4
27 1 ↵G. Wulff, *Z. Krystallog.* 34, 449 (1901).OpenUrl
28 1 E. Ringe, R. P. Van Duyne, L. D. Marks, Wulff construction for alloy nanoparticles. *Nano Lett.* 11, 3399–3403 (2011). doi:10.1021/nl2018146 pmid:21744799
29 1 ↵S. Polarz, Shape matters: Anisotropy of the morphology of inorganic colloidal particles - synthesis and function. *Adv. Funct. Mater.* 21,

3214–3230 (2011). doi:10.1002/adfm.201101205
30 1 ↵P. J. Eng, T. P. Trainor, G. E. Brown Jr, G. A. Waychunas, M. Newville, S. R. Sutton, M. L. Rivers, Structure of the hydrated alpha-Al(2)O(3) (0001) surface. *Science* 288, 1029–1033 (2000). doi:10.1126/science.288.5468.1029 pmid:10807569
31 1 P. J. Feibelman, Partial dissociation of water on Ru(0001). *Science* 295, 99–102 (2002). doi:10.1126/science.1065483 pmid:11778041
32 1 S. U. Khan, M. Al-Shahry, W. B. Ingler Jr., Efficient photochemical water splitting by a chemically modified n-TiO2. *Science* 297, 2243–2245 (2002). doi:10.1126/science.1075035 pmid:12351783
33 1 ↵H. J. Shin, J. Jung, K. Motobayashi, S. Yanagisawa, Y. Morikawa, Y. Kim, M. Kawai, State-selective dissociation of a single water molecule on an ultrathin MgO film. *Nat. Mater.* 9, 442–447 (2010). doi:10.1038/nmat2740 pmid:20400956
34 1 ↵W. T. Pong, C. Durkan, A review and outlook for an anomaly of scanning tunnelling microscopy (STM): Superlattices on graphite. *J. Phys. D Appl. Phys.* 38, R329–R355 (2005). doi:10.1088/0022-3727/38/21/R01
35 1 ↵S. Wu, R. Yang, D. Shi, G. Zhang, Identification of structural defects in graphitic materials by gas-phase anisotropic etching. *Nanoscale* 4, 2005–2009 (2012). doi:10.1039/c2nr11707j pmid:22318671
36 1 ↵X. Deng, A. Verdaguer, T. Herranz, C. Weis, H. Bluhm, M. Salmeron, Surface chemistry of Cu in the presence of CO2 and H2O. *Langmuir* 24, 9474–9478 (2008). doi:10.1021/la8011052 pmid:18646877
37 1 ↵K. Andersson, A. Nikitin, L. Pettersson, A. Nilsson, H. Ogasawara, Water dissociation on Ru(001): An activated process. *Phys. Rev. Lett.* 93, 196101 (2004). doi:10.1103/PhysRevLett.93.196101 pmid:15600853
38 1 ↵G. Kresse, J. Hafner, Ab initio molecular dynamics for liquid metals. *Phys. Rev. B* 47, 558–561 (1993). doi:10.1103/PhysRevB.47.558
39 1 G. Kresse, J. Hafner, Ab initio molecular-dynamics simulation of the liquid-metal–amorphous-semiconductor transition in germanium. *Phys. Rev. B* 49, 14251–14269 (1994). doi:10.1103/PhysRevB.49.14251
40 1 G. Kresse, J. Furthmüller, Efficiency of ab-initio total energy calculations for metals and semiconductors using a plane-wave basis set. *Comput. Mater. Sci.* 6, 15–50 (1996). doi:10.1016/0927-0256(96)00008-0
41 1 G. Kresse, J. Furthmüller, Efficient iterative schemes for ab initio total-energy calculations using a plane-wave basis set. *Phys. Rev. B* 54, 11169–11186 (1996). doi:10.1103/PhysRevB.54.11169
42 1 G. Kresse, D. Joubert, From ultrasoft pseudopotentials to the projector augmented-wave method. *Phys. Rev. B* 59, 1758–1775 (1999). doi:10.1103/PhysRevB.59.1758
43 J. Perdew, P. Ziesche, H. Eschrig, Eds., *Electronic Structure of Solids '91* (Akademie Verlag, Berlin, 1991).
44 1 J. Perdew, Y. Wang, Accurate and simple analytic representation of the electron-gas correlation energy. *Phys. Rev. B* 45, 13244–13249 (1992). doi:10.1103/PhysRevB.45.13244
45 1 J. Perdew, K. A. Jackson, M. R. Pederson, D. J. Singh, C. Fiolhais,

Atoms, molecules, solids, and surfaces: Applications of the generalized gradient approximation for exchange and correlation. *Phys. Rev. B* 46, 6671–6687 (1992). doi:10.1103/PhysRevB.46.6671
46 1 P. E. Blöchl, Projector augmented-wave method. *Phys. Rev. B* 50, 17953–17979 (1994). doi:10.1103/PhysRevB.50.17953
47 1 E. Davidson, *NATO Advanced Study Institute, Series C* 113, 95 (1983)
48 1 H. Monkhorst, J. Pack, Special points for Brillouin-zone integrations. *Phys. Rev. B* 13, 5188–5192 (1976). doi:10.1103/PhysRevB.13.5188
49 1 K. Momma, F. J. Izumi, *VESTA*: A three-dimensional visualization system for electronic and structural analysis. *J. Appl. Cryst.* 41, 653–658 (2008). doi:10.1107/S0021889808012016
50 1 K. Momma, F. J. Izumi, *VESTA 3* for three-dimensional visualization of crystal, volumetric and morphology data. *Appl. Cryst.* 44, 1272–1276 (2011). doi:10.1107/S0021889811038970
51 M. D. Hanwell *et al.*, *J. Cheminf.* 4 (2012).
52 1 Y. Noda, K. Masumoto, S. Ohba, Y. Saito, K. Toriumi, Y. Iwata, I. Shibuya, Temperature dependence of atomic thermal parameters of lead chalcogenides, PbS, PbSe and PbTe. *Acta Crystallogr. C* 43, 1443–1445 (1987). doi:10.1107/S0108270187091509
53 1 Y. Gai, H. Peng, J. Li, Electronic properties of nonstoichiometric PbSe quantum dots from first principles. *J. Phys. Chem. C* 113, 21506–21511 (2009). doi:10.1021/jp905868f
54 1 X. Huang, E. Lindgren, R. Chelikowsky, Surface passivation method for semiconductor nanostructures. *Phys. Rev. B* 71, 165328 (2005). doi:10.1103/PhysRevB.71.165328
55 1 C. B. Duke, Semiconductor surface reconstruction: The structural chemistry of two-dimensional surface compounds. *Chem. Rev.* 96, 1237–1260 (1996). doi:10.1021/cr950212s pmid:11848788
56 1 J. Chen, C. L. Brooks 3rd, H. A. Scheraga, Revisiting the carboxylic acid dimers in aqueous solution: Interplay of hydrogen bonding, hydrophobic interactions, and entropy. *J. Phys. Chem. B* 112, 242–249 (2008). doi:10.1021/jp074355h pmid:17880128
57 1 M. Hines, G. Scholes, Colloidal PbS nanocrystals with size-tunable near-infrared emission: Observation of post-synthesis self-narrowing of the particle size distribution. *Adv. Mater.* 15, 1844–1849 (2003). doi:10.1002/adma.200305395
58 1 A. Satta, S. de Gironcoli, Surface structure and core-level shifts in lead chalcogenide (001) surfaces. *Phys. Rev. B* 63, 033302 (2000). doi:10.1103/PhysRevB.63.033302
59 1 J. Muscat, J. Gale, First principles studies of the surface of galena PbS. *Geochim. Cosmochim. Acta* 67, 799–805 (2003). doi:10.1016/S0016-7037(02)00978-X
60 1 J.-X. Ma, Y. Jia, Y.- Song, E.- Liang, L.- Wu, F. Wang, X.- Wang, X. Hu, The geometric and electronic properties of the PbS, PbSe and PbTe (001) surfaces. *Surf. Sci.* 551, 91–98 (2004). doi:10.1016/j.susc.2003.12.003

61 1 P. Boher, P. Garnier, J. R. Gavarri, A. W. Hewat, Monoxyde quadratique PbOα(I): Description de la transition structurale ferroe´lastique. *J. Solid State Chem*. 57, 343–350 (1985). doi:10.1016/0022-4596(85)90197-5
62 1 A. Coolidge, The vapor density and some other properties of formic acid. *J. Am. Chem. Soc*. 50, 2166–2178 (1928). doi:10.1021/ja01395a015
63 1 R. Millikan, K. Pitzer, The infrared spectra of dimeric and crystalline formic acid. *J. Am. Chem. Soc*. 80, 3515–3521 (1958). doi:10.1021/ja01547a007
64 1 M. E. Dunn, T. M. Evans, K. N. Kirschner, G. C. Shields, Prediction of accurate anharmonic experimental vibrational frequencies for water clusters, (H2O)n, n=2-5. *J. Phys. Chem. A* 110, 303–309 (2006). doi:10.1021/jp054958y pmid:16392869
65 1 A. Vítek, R. Kalus, I. Paidarová, Structural changes in the water tetramer. A combined Monte Carlo and DFT study. *Phys. Chem. Chem. Phys*. 12, 13657–13666 (2010). doi:10.1039/c0cp00217h pmid:20852812
66 1 J. F. Boily, J. Szanyi, A. R. Felmy, A combined FTIR and TPD study on the bulk and surface dehydroxylation and decarbonation of synthetic goethite. *Geochim. Cosmochim. Acta* 70, 3613–3624 (2006). doi:10.1016/j.gca.2006.05.013
67 1 J. Ceponkus, P. Uvdal, B. Nelander, Water tetramer, pentamer, and hexamer in inert matrices. *J. Phys. Chem. A* 116, 4842–4850 (2012). doi:10.1021/jp301521b pmid:22533460
68 1 J. B. Brown, G. Y. Shinowara, Studies on the chemistry of the fatty acids. II. The preparation of pure oleic acid by a simplified method. *J. Am. Chem. Soc*. 59, 6–8 (1937). doi:10.1021/ja01280a003
69 1 M. H. Brooker, S. Sunder, P. Taylor, V. J. Lopata, Infrared and Raman spectra and X-ray diffraction studies of solid lead(II) carbonates. *Can. J. Chem*. 61, 494–502 (1983). doi:10.1139/v83-087
70 1 J. M. Krier, W. D. Michalak, L. R. Baker, K. An, K. Komvopoulos, G. A. Somorjai, Sum Frequency Generation Vibrational Spectroscopy of Colloidal Platinum Nanoparticle Catalysts: Disordering versus Removal of Organic Capping. *J. Phys. Chem. C* 116, 17540–17546 (2012). doi:10.1021/jp303363m
71 1 X. Wang, L. Andrews, Infrared spectra of M(OH)(1,2,4) (M = Pb, Sn) in solid argon. *J. Phys. Chem. A* 109, 9013–9020 (2005). doi:10.1021/jp053420p pmid:16332006
72 1 F. Rueda, J. Mendialdua, A. Rodriguez, Y. R.Casanova, L. Barbaux, L. Gengembre, Jalowiecki, Characterization of Venezuelan laterites by X-ray photoelectron spectroscopy. *J. Electron Spectrosc. Relat. Phenom*. 82, 135–143 (1996). doi:10.1016/S0368-2048(96)03035-6
73 1 J. A. Th. Verhoeven, H. Van Doveren, An XPS investigation of the interaction of CH4, C2H2, C2H4 and C2H6 with a barium surface. *Surf. Sci*. 123, 369–383 (1982). doi:10.1016/0039-6028(82)90334-X
74 1 T. Sugama, L. E. Kukacka, N. Carciello, N. J. Hocker, Study of interactions at water-soluble polymer/Ca(OH)2 or gibbsite interfaces by XPS. *Cement Concr. Res*. 19, 857–867 (1989). doi:10.1016/0008-8846(89)90098-7

75 1 J. Haber, J. Stoch, L. Ungier, X-ray photoelectron spectra of oxygen in oxides of Co, Ni, Fe and Zn. *J. Electron Spectrosc.* 9, 459–467 (1976). doi:10.1016/0368-2048(76)80064-3
76 1 N. S. McIntyre *et al.*, Chemical information from XPS—applications to the analysis of electrode surfaces. *J. Vac. Sci. Technol.* 18, 714 (1981). doi:10.1116/1.570934
77 1 A. M. Venezia, R. Bertoncello, G. Deganello, X-ray photoelectron spectroscopy investigation of pumice-supported nickel catalysts. *Surf. Interface Anal.* 23, 239–247 (1995). doi:10.1002/sia.740230408
78 1 T. Dickinson, A. F. Povey, P. M. A. Sherwood, X-ray photoelectron spectroscopic study of the film formed on a gold electrode during the electrochemical reduction of chromium(VI). *J. Chem. Soc., Faraday Trans.* 72, 686 (1976). doi:10.1039/f19767200686
79 1 F. Bournel, C. Laffon, Ph. Parent, G. Tourillon, Adsorption of some substituted ethylene molecules on Pt(111) at 95 K Part 1: NEXAFS, XPS and UPS studies. *Surf. Sci.* 350, 60–78 (1996). doi:10.1016/0039-6028(95)01254-0
80 1 J. Podlahová, L. Kavan, J. Šilha, J. Podlaha, Nickel(II) complexes of ethylenediphosphinetetra-acetic acid. *Polyhedron* 3, 963–968 (1984). doi:10.1016/S0277-5387(00)84653-7
81 1 S. B. Amor, M. Jacquet, P. Fioux, M. Nardin, XPS characterisation of plasma treated and zinc oxide coated PET. *Appl. Surf. Sci.* 255, 5052–5061 (2009). doi:10.1016/j.apsusc.2008.12.067
82 1 K. B. Yatsimirskii, V. V. Nemoskalenko, V. G. Aleshin, Y. I. Bratushko, E. P. Moiseenko, X-ray photoelectron spectra of mixed oxygenated cobalt(II)-amino acid-imidazole complexes. *Chem. Phys. Lett.* 52, 481–484 (1977). doi:10.1016/0009-2614(77)80490-9
83 1 ↵A. Centrone, Y. Hu, A. M. Jackson, G. Zerbi, F. Stellacci, Phase separation on mixed-monolayer-protected metal nanoparticles: a study by infrared spectroscopy and scanning tunneling microscopy. *Small* 3, 814–817 (2007). doi:10.1002/smll.200600736 pmid:17410617
84 Acknowledgments: We thank R. Cai and Z. Zhu for helpful discussions and J. Engel for help in the XPS experiments. This work was supported by the Director, Office of Science, the Office of Basic Energy Sciences (BES), Materials Sciences and Engineering (MSE) Division of the U.S. Department of Energy (DOE) through the organic/inorganic nanocomposite program under contract DE-AC02-05CH11231. It used resources of the National Energy Research Scientific Computing Center, the Molecular Foundry, and the Advance Light Source, which are supported by the Office of Science of the U.S. Department of Energy. Computations also used resources of the Oak Ridge Leadership Computing Facility at the Oak Ridge National Laboratory, which is supported by the Office of Science of the U.S. Department of Energy under contract no. DE-AC05-00OR22725, with computational time allocated by the Innovative and Novel Computational Impact on Theory and Experiment (INCITE) project. M.S. would like to thank the Alexander von Humboldt-Foundation for a Feodor Lynen-Fellowship. Materials and methods, supporting information, and coordinates of

NC models are included in the supplementary materials.